

Electrical Tuning of Plasmonic Conducting Polymer Nanoantennas

Akchheta Karki, Giancarlo Cincotti, Shangzhi Chen, Vallery Stanishev, Vanya Darakchieva, Chuanfei Wang, Mats Fahlman, and Magnus P. Jonsson*

Nanostructures of conventional metals offer manipulation of light at the nanoscale but are largely limited to static behavior due to fixed material properties. To develop the next frontier of dynamic nano-optics and metasurfaces, this study utilizes the redox-tunable optical properties of conducting polymers, as recently shown to be capable of sustaining plasmons in their most conducting oxidized state. Electrically tunable conducting polymer nano-optical antennas are presented, using nanodisks of poly(3,4-ethylenedioxythiophene:sulfate) (PEDOT:Sulf) as a model system. In addition to repeated on/off switching of the polymeric nanoantennas, the concept enables gradual electrical tuning of the nano-optical response, which was found to be related to the modulation of both density and mobility of the mobile polaronic charge carriers in the polymer. The resonance position of the PEDOT:Sulf nanoantennas can be conveniently controlled by disk size, here reported down to a wavelength of around 1270 nm. The presented concept may be used for electrically tunable metasurfaces, with tunable farfield as well as nearfield. The work thereby opens for applications ranging from tunable flat meta-optics to adaptable smart windows.


nanostructures are limited as it has proven unduly challenging to modify their static properties after fabrication.^[19] To circumvent this major issue and open avenues to dynamically control light at the nanoscale, research is shifting toward dynamic systems with tunable properties, for example, based on phase change materials,^[20–24] doped metal oxide nanocrystals,^[25] and graphene.^[26–28] Motivated by an exceptionally large redox-tunability,^[29] we recently introduced conducting polymers as a new materials platform for dynamic plasmonics.^[30] Conducting polymers have been previously used to modulate plasmonic responses of nanostructures made of conventional metals like gold.^[31–34] We showed that nanodisks of the highly conducting polymer poly(3,4-ethylenedioxythiophene:sulfate) (PEDOT:Sulf) can function as dynamic plasmonic nanoantennas also without any metallic nanostructures, with the polymer

itself being the plasmonic material owing to its highly mobile and large density of polaronic charge carriers ($2.6 \times 10^{21} \text{ cm}^{-3}$, determined by ellipsometry).^[30] Excitingly, these nanoantennas could be completely switched on and off by chemical tuning of the polymer's redox state, which dramatically modulates the conductivity and optical properties of the material.^[30] However, the tuning process was based on exposure to gases and liquids while future systems will require more convenient and faster electrical tuning.

1. Introduction

Metal nanostructures can be used as optical nanoantennas by converting free-space optical radiation into collective charge oscillations called plasmons.^[1] Due to their ability to control light at the nanoscale, such systems have been utilized in areas including energy conversion,^[2–4] biosensing,^[5–9] display technologies,^[10–13] and ultrathin optical components.^[14–18] However, light–matter interactions with conventional metal

A. Karki, G. Cincotti, S. Chen, C. Wang, M. Fahlman, M. P. Jonsson
Laboratory of Organic Electronics
Department of Science and Technology (ITN)
Linköping University
Norrköping SE-601 74, Sweden
E-mail: magnus.jonsson@liu.se

 The ORCID identification number(s) for the author(s) of this article can be found under <https://doi.org/10.1002/adma.202107172>.

© 2022 The Authors. Advanced Materials published by Wiley-VCH GmbH. This is an open access article under the terms of the Creative Commons Attribution-NonCommercial License, which permits use, distribution and reproduction in any medium, provided the original work is properly cited and is not used for commercial purposes.

DOI: 10.1002/adma.202107172

V. Stanishev, V. Darakchieva
Terahertz Materials Analysis Center (TheMAC)
Department of Physics
Chemistry and Biology (IFM)
Linköping University
Linköping SE-581 83, Sweden
V. Stanishev, V. Darakchieva
Center for III-Nitride Technology
C3NiT-Janzèn
Department of Physics
Chemistry and Biology (IFM)
Linköping University
Linköping SE-581 83, Sweden
V. Darakchieva
Solid State Physics and NanoLund
Lund University
Lund S-221 00, Sweden

In this work, we take the next crucial step in the study of conducting polymer plasmonics and present electrically tunable conducting polymer optical nanoantennas. Using PEDOT:Sulf nanodisks as a model system, we demonstrate repeatable and complete on/off switching by electrochemically switching the polymer between its highly conducting plasmonic oxidized state and a lower conducting dielectric reduced state. In addition, we demonstrate electrically controlled gradual tuning of the plasmonic response by gradual modulation of the polymer redox state. Complementary analytical calculations and simulations suggest that the tunable response originates from modulation of both density and mobility of the mobile polaronic charge carriers in the polymer. The combination of gradual tuning of the nanoantennas and the ability to turn them completely on and off enables many future applications in the direction of dynamic nano-optics and metasurfaces, such as smart windows with controllable plasmon-induced heating, bio-applications with NIR bio-windows,^[35] and dynamic ultrathin optical components for beam steering or lensing with tunable focal length.^[36,37]

2. Results and Discussions

Figure 1a shows the chemical structures of PEDOT:Sulf in its oxidized (plasmonic) and reduced (dielectric) states, which form

the basis for its use as a dynamic plasmonic material. Figure 1b compares the in-plane permittivity of PEDOT:Sulf in the two states, indeed showing a clear transition between metallic (negative real permittivity) and dielectric (positive real permittivity) response. The data for the oxidized state was obtained from our previous work^[30] and we measured the permittivity of chemically reduced PEDOT films (Figures S1–S3 and Table S1, Supporting Information, contain the raw ellipsometry data, fitting parameters, and the out-of-plane permittivity). The oxidized PEDOT:Sulf film provides negative real permittivity and a lower magnitude imaginary permittivity in the spectral region from 0.8–3.6 μm , which was defined as the plasmonic regime.^[30] Contrastingly, the reduced material instead largely shows positive permittivity in the same spectral region, presenting an opportunity to tune PEDOT:Sulf-based systems between its plasmonic and dielectric behavior. Indeed, simulations using experimentally obtained material properties for the oxidized and reduced states demonstrate the potential for tuning both farfield and nearfield responses of PEDOT:Sulf nanoantennas. The blue curve in Figure 1c shows the optical extinction of an oxidized (plasmonic) PEDOT:Sulf nanodisk array, exhibiting a clear resonance peak at a wavelength of around 1500 nm. By contrast, this resonance peak is not present for the same nanodisk array made of the chemically reduced (dielectric) PEDOT (black curve). Instead, there are two peaks at wavelengths of

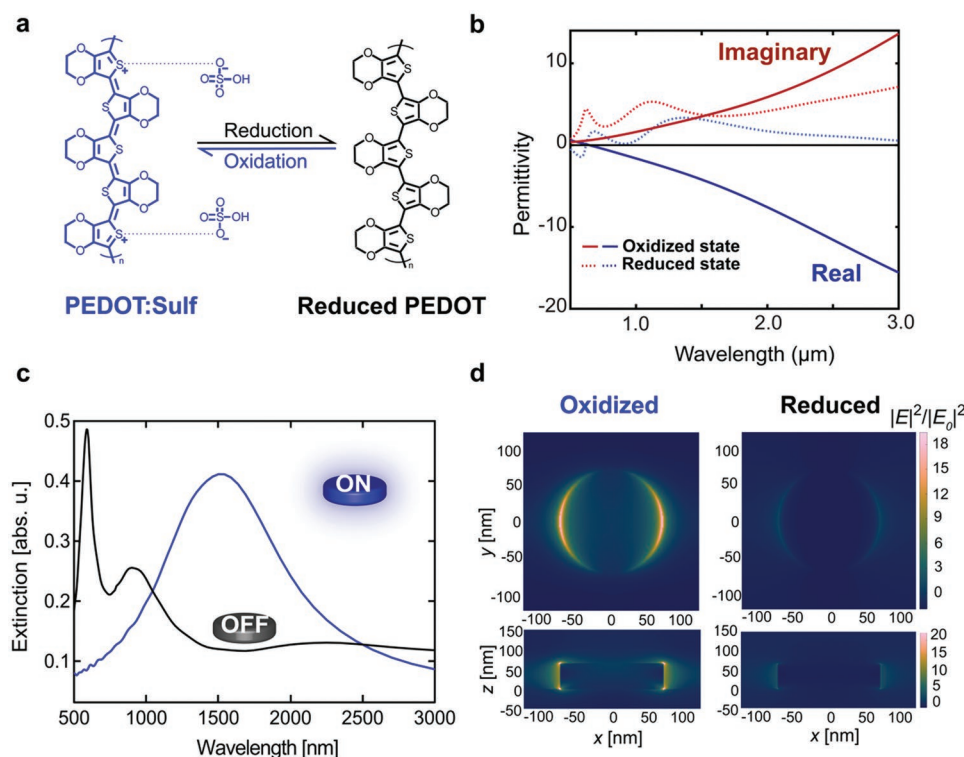


Figure 1. Concept of electrically tunable conducting polymer nanoantennas. a) Molecular structures of PEDOT:Sulf in its oxidized (plasmonic) and reduced (dielectric) states. b) In-plane permittivity dispersion of PEDOT:Sulf in its oxidized (blue curve, real part; red curve, imaginary part) and reduced (dashed blue curve, real part; dashed red curve, imaginary part) states.^[30] c,d) Simulated extinction (c) and nearfield response (d) for nanodisk arrays (diameter = 145 nm, thickness = 65 nm, period = 600 nm) at the resonance peak wavelength of ≈ 1500 nm, based on fully oxidized (blue) and chemically reduced (black) PEDOT:Sulf. In (d), the top panels are top views while the bottom panels are cross sections of the nanodisks along the direction of the incident polarization, which is along the x-axis. The x–y in-plane direction is 2 nm above the nanodisk and the x–z cross section is through the center of the nanodisk. The color scale bars show the square of the electric field strength relative to the incident light ($|E|^2/|E_0|^2$).

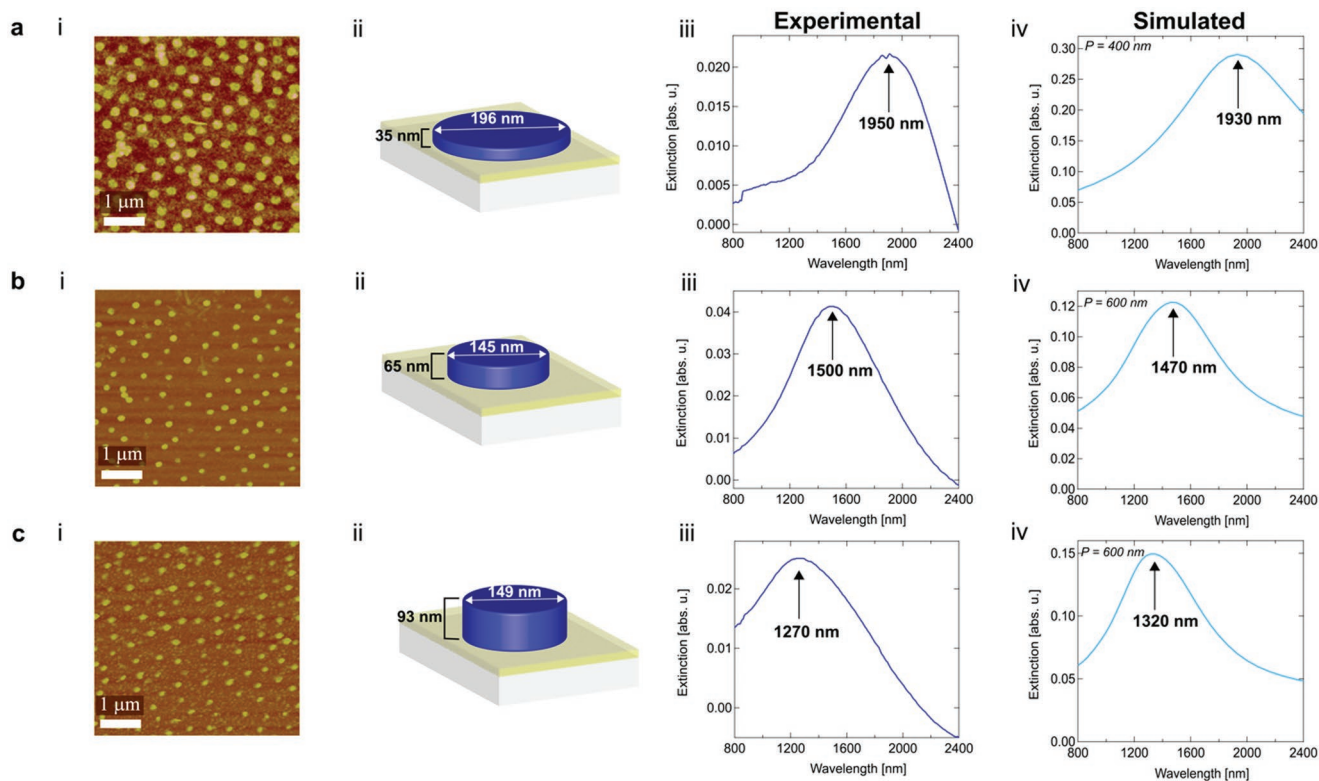


Figure 2. Resonance-tuning by nanodisk geometry. a–c) Nanodisks made using one (a), two (b), and three (c) PEDOT:Sulf layers to control the thickness, with (i) AFM images, (ii) a schematic of the nanodisks with the extracted dimensions from the AFM height and width analyses. (iii) Experimental extinction spectra and (iv) simulated extinction spectra for nanodisks of the corresponding dimensions on glass. The different values of P indicated in each panel in (iv) correspond to the array period in the periodic simulations.

≈ 1000 and ≈ 630 nm, which are attributed to the low oxidation and neutral states of PEDOT, respectively.^[38] As the oxidized state of PEDOT is more stable in air than the neutral state, we observe a small signature peak at ≈ 1000 nm from its lower oxidation state. The simulated data is comparable to the experimentally obtained extinction spectra of oxidized and reduced PEDOT:Sulf nanodisks, as presented in Figure S4, Supporting Information. Figure 1d compares the optical near-field profiles of the oxidized and reduced states of a nanodisk (at the resonance wavelength of ≈ 1500 nm), demonstrating that the intensity of the enhanced electric fields around the nanoantenna is significantly higher in the oxidized state, thereby confirming the expected tunability also of the nearfield nanoantenna response. Interestingly, we observe only a rather small influence of the permittivity of the polymer being strongly anisotropic, although this property may be explored and utilized further in future systems (see Figure S5 and Note S1, Supporting Information).

To experimentally confirm excitation of plasmons in PEDOT:Sulf polymer nanodisks and demonstrate spectral control of their plasmonic response, we fabricated sparse arrays of nanodisks of different dimensions on sputtered indium tin oxide (ITO) substrates using colloidal lithography (detailed schematic of the polymerization and colloidal lithography process can be found in Figure S6, Supporting Information). Atomic force microscopy (AFM) images reveal successful fabrication of large areas of nanodisks (Figure 2a–i–c-i). Height and width section analyses of individual nanodisks from AFM

images (Figures S7–S9, Supporting Information) were used to extract the representative heights and diameters, as presented in Figure 2a–i–c-ii. Our previous work established that decreasing the diameter of the nanodisks could blueshift the resonance peaks, whereby resonance peaks down to 1800 nm were attained for around 30 nm thick PEDOT.^[30] In this work, we instead limited the variation in nanodisk diameter (149–196 nm) and increased the thickness of the nanodisks, leading to significantly blueshifted peaks, with lowest resonance wavelength of around 1270 nm. This is the lowest resonance wavelength reported so far for conducting polymer nanoantennas. By sequentially increasing the nanodisk thickness from ≈ 30 nm (based on one layer of vapor phase polymerized [VPP] PEDOT:Sulf), to ≈ 60 nm (two layers of VPP PEDOT:Sulf), and finally ≈ 90 nm (three layers of VPP PEDOT:Sulf), we achieved substantial blueshifts in the experimental resonance peaks, from ≈ 1950 nm down to ≈ 1270 nm (Figure 2a-iii–c-iii) for around 150 nm in diameter nanodisks. The small variations in nanodisk diameter are related to separate optimization of the polymer etching time for the three different film thicknesses. Comparison with nanodisks on glass substrates shows that the ITO does not significantly affect the plasmonic resonances, although with a tendency to blueshift and lower the intensity of the extinction peaks (Figure S10, Supporting Information). Experimental results match simulated results for nanodisks on glass in terms of both peak wavelengths and peak widths (Figure 2a-iv–c-iv). Discrepancies can be attributed

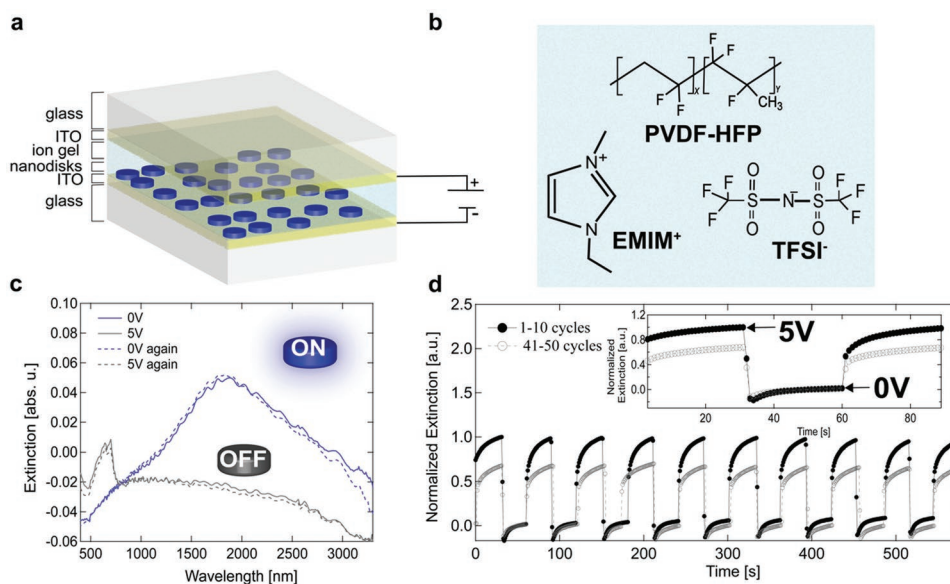


Figure 3. Reversible electrical on/off switching of PEDOT:Sulf nanoantennas. a) Schematic illustration of the electrically tunable device, based on conducting polymer nanodisks on an ITO electrode, electrochemically modulated via a transparent ion gel and a second top ITO electrode. b) Chemical structures of the components in the ion gel. c) Extinction spectra for a device with 145 nm in diameter and 65 nm thick nanodisks at 0 and 5 V, with dashed lines showing excellent reversibility upon repeated switching. The small undulations are attributed to optical interference in the thin-film device structure due to the sandwiched ion gel, as also observed without the nanodisks (Figure S12a, Supporting Information) and previously reported for similar ion gel components and device structures as used in this work.^[43] d) Normalized extinction at the plasmonic peak position of around 1800 nm over time during multiple (50) switching cycles, with the inset showing results for the 1st and 41st cycles.

to geometrical variations, inaccuracies in permittivities, differences in substrates, and imperfections of the fabricated nanodisks and their coverage on the substrate. The large resonance blueshift, using only minor modifications in geometry, is promising for achieving resonances also in the visible spectral range, especially in combination with further materials optimization.

Regarding the sometimes negative extinction values observed at longer wavelengths, we note that the extinction is presented using a sputtered ITO/glass substrate as the reference. Negative values therefore mean that the sample with nanoantennas transmitted more light than the reference substrate in that wavelength range. This can occur due to natural variations between the sputtered ITO/glass substrates. Indeed, extinction baseline shifts appeared also when measuring a substrate without nanoantennas using another equivalent substrate without nanoantennas as the reference (Figure S11, Supporting Information). In addition, we cannot exclude possible contribution to lowered extinction values due to the nanoantennas aiding light transmission, for example, by reducing reflection at the air/sample interface. Both experiments and simulations indicate that the nanodisks may reduce the reflectance at longer wavelengths (Figures S15a,b and S16, Supporting Information), although this does not need to lead to negative extinction values (Figure S15c,d, Supporting Information).

Next, we demonstrate electrical switching of the conducting polymer nanoantenna surfaces. We here utilize that the redox state of conducting polymers can be modulated electrochemically.^[39–43] Figure 3a shows the basic device structure, based on PEDOT:Sulf nanodisks on an ITO/glass substrate, coated by an ion gel followed by a second ITO/glass substrate. The two ITO layers act as electrodes and are separated by the ion

gel containing the ionic liquid 1-ethyl-3-methylimidazolium bis(trifluoromethylsulfonyl)imide ([EMIM⁺][TFSI⁻]) in a mixture of the copolymer poly[(vinylidene fluoride)-*co*-hexafluoropropylene] (PVDF-HFP) in acetone. Figure 3b shows the chemical structures of the components in the ion gel, which provide high transparency in the visible to mid-IR ranges (see Figure S12a, Supporting Information). It is worth noting that applying the ion gel on top of the nanodisks redshifted the plasmonic resonance (Figure S12b, Supporting Information), as expected due to the increase in refractive index of the surrounding medium from 1 ($n_{\text{air}} = 1$) to that of the ion gel ($n_{\text{ion-gel}} \approx 1.42$).^[44–46]

Figure 3c shows extinction spectra of a complete device using an equivalent reference device without nanoantennas as reference. The results demonstrate that the resonance peak observed in the oxidized plasmonic state (at 0 V, blue curve) could be completely suppressed by applying a positive bias of 5 V from the top ITO electrode, which reduces the polymer and effectively turns off the nanoantennas (gray curve) on the bottom electrode. As for the measurements in air, the negative extinction values are also here primarily attributed to variations in transmission between the nanoantenna device and the assembled reference device (glass–ITO/ion gel/ITO–glass, see Figure S13, Supporting Information). Figure S14, Supporting Information, reports switching data for another similar nanoantenna device that instead mostly shows positive values in the same region, yet with tendency of negative values toward longer wavelengths which may be related to the presence of the nanoantennas (see Figures S15 and S16, Supporting Information).

For our switching experiments, the bottom electrode containing the polymer antennas was grounded, so applying a

5 V bias from the top ITO electrode is equivalent to applying a -5 V bias to the bottom ITO electrode (dashed line, see confirmation in Figure S17, Supporting Information). The nanoantennas could be switched on again by applying a 0 V potential and thereby re-oxidizing the material to make it plasmonic again (dashed blue curve). To better understand the switching behavior, we note that the PEDOT:Sulf nanodisks are in their oxidized state at 0 V, with high density mobile polaronic charge carriers giving rise to the plasmonic response. At this state, the mobile positive polaronic charges in the PEDOT:Sulf nanodisks are being compensated by the sulfate counterions (HSO_4^-) as depicted in Figure 1a. Upon applying a positive bias from the top ITO electrode via the ion gel, cations (EMIM^+) from the ion gel get injected into the polymer nanodisks, which are compensated by the HSO_4^- anions.^[43] The presence of EMIM^+ in the PEDOT:Sulf film after applying a positive bias was confirmed by X-ray photoelectron spectroscopy (XPS), showing clear nitrogen signals due to the N and N^+ signals present in EMIM^+ (Figure S18a, Supporting Information). Additionally, the sulfur signal from HSO_4^- moved toward higher binding energies after switching, which could be an indication of the sulfur from HSO_4^- coordinating with N^+ from the cation EMIM^+ rather than with the positive polaronic charge carriers in PEDOT:Sulf (as in the oxidized state) (Figure S18b, Supporting Information). Consequently, applying a positive bias decreases the density of holes in the PEDOT:Sulf due to the lack of coordination between HSO_4^- and the positive polaronic charge carriers in the polymer film.^[43] As a result, the polymer nanoantennas reach an off state where the density of mobile polaronic charge carriers are so low that the film no longer exhibits plasmonic behavior, as shown by the gray curves in Figure 3c.

To further understand the dynamics of the switching process, we monitored the optical extinction (normalized from zero to one relative to the first switching cycle) at the plasmonic peak position of around 1800 nm in real time while repeatedly switching the bias between 0 and 5 V (Figure 3d). The results show reversible transitions between the on (0 V) and off (5 V) states for at least 50 switching cycles (50 min) (see results for all cycles in Figure S19, Supporting Information), albeit with some reduction in the extinction values after many cycles. The inset in Figure 3d shows that it took only a few seconds for the nanodisk extinction signal to reach the off state after applying the bias, and a further 20–30 s for the values to fully stabilize. Likewise, it took about 20–30 s for the extinction values to stabilize after turning the nanoantennas on again (i.e., removing the bias). These values, which are based on devices not optimized for speed, are in line with typical conducting polymer electrochemical devices with similar solid ion gel-based electrolytes.^[43,46,47] Because the switching speed is strongly dependent on the mobility of the ions in the solid ion gel, there is potential for further improvements by optimizing the electrolyte to obtain higher ionic mobility.^[43,47,49] Furthermore, recent research also showed that modified device configurations and use of aqueous electrolytes can boost the switching speed of conducting polymer devices even to video rates.^[50]

We will now demonstrate that the plasmonic response of conducting polymer nanoantennas can be tuned gradually, in addition to complete electrical on/off switching. Figure 4a shows experimental extinction spectra at different biases applied from

the top ITO electrode, for a device with 145 nm in diameter and 65 nm thick PEDOT:Sulf nanodisks. The results show gradual suppression of the nanoantenna response accompanied by a small redshift of the extinction peak position. The gradual tuning was also reversible, as demonstrated in Figure S20, Supporting Information. Similar results were obtained for PEDOT:Sulf nanodisks with other thicknesses (Figure S21, Supporting Information).

During the gradual tuning process, the PEDOT:Sulf nanodisks evolve toward a reduced state with increasing applied bias, as confirmed by the appearance of a peak at ≈ 1000 nm at 3 V related to the lower oxidation state of PEDOT.^[38] Upon further increasing the bias to 5 V, a peak at ≈ 630 nm originates from the reduced neutral PEDOT.^[38] In this reduced state, any signs of plasmons originating from the mobile polaronic charges have been diminished as a result of polymer reduction. Control measurements using the same device configuration as used for the nanodisks but with a nonstructured PEDOT:Sulf film confirm that the polymer is gradually reduced with an increasing bias (Figure S22, Supporting Information), including reduction of the IR absorbance and emergence of the neutral (≈ 600 nm) and polaronic (≈ 1000 nm) peaks. While reduction of the PEDOT:Sulf nanodisks was not clearly visible by eye, the reduced PEDOT:Sulf film also took on its traditional deeper blue coloration (Figure S22b, Supporting Information).^[51–54]

To better understand the dynamic nano-optical response of the PEDOT nanoantennas and the relation to changes in the polaronic charge transport at different biases, we calculated their extinction cross section ($\sigma(\lambda)$) using dipolar polarizability theory and by varying the in-plane polymer permittivity ($\epsilon(\lambda)$) via changes in the charge carrier mobility and/or concentration. Treating the nanodisks as oblate spheroids with diameter D and thickness t , the polarizability (α) in the quasi-static limit ($D \ll \lambda$) is given by:^[55]

$$\alpha(\lambda) = V \frac{\epsilon(\lambda) - \epsilon_s}{\epsilon_s + L[\epsilon(\lambda) - \epsilon_s]} \quad (1)$$

where V is the volume of the spheroid, L is a geometrical factor that depends on spheroid aspect ratio, and ϵ_s is the permittivity of the surrounding medium (set to 2.13 to resemble the effective surrounding permittivity for disks surrounded by the ion gel on a glass substrate). As larger disks require correction for finite wavelength effects, we further correct the polarizability using:^[56,57]

$$\alpha'(\lambda) = \alpha(\lambda) \left[1 - \frac{k^2}{2\pi D} \alpha(\lambda) - i \frac{k^3}{6\pi} \alpha(\lambda) \right]^{-1} \quad (2)$$

where k is the wavenumber of the incident light and i is the imaginary number. The extinction cross section $\sigma(\lambda)$ of the nanodisks/spheroids can now be calculated as:

$$\sigma(\lambda) = k \text{Im}[\alpha'(\lambda)] \quad (3)$$

The black curves in Figure 4b–d show the calculated extinction for a fully oxidized PEDOT:Sulf nanodisk, with good agreement with the experimental results (Figure 4a) in terms of both resonance position and peak width. $\epsilon(\lambda)$ was here

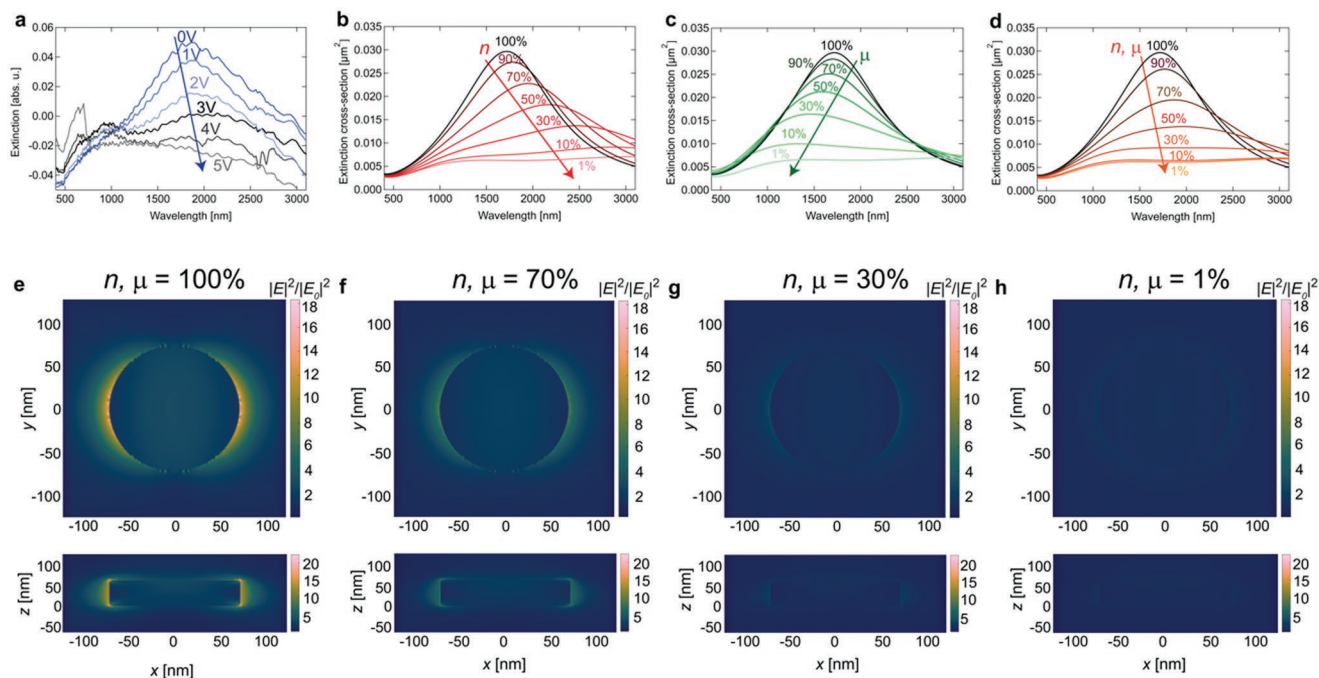


Figure 4. Gradual electrical tuning of conducting polymer nanoantennas. a) Experimental extinction results at different biases, showing the capability of gradual tuning of the nanoantenna response for a device with 145 nm in diameter and 65 nm thick PEDOT:Sulf nanodisks. b–d) Calculated extinction based on dipolar polarizability theory of the nanodisks treated as oblate spheroids (same dimensions as in (a)), with material properties varying from the fully oxidized material by gradually decreasing carrier density (b), carrier mobility (c), both carrier density and mobility (d). e–h) Simulated nearfields for a single nanodisk on glass (same dimensions as in (a)) at the resonance peak with jointly varying carrier density and mobility, from 100% (fully oxidized) (e), reduction to 70% of both carrier density and mobility (f), reduction to 30% (g), and reduction to 1% (h) of the original carrier density and mobility. The color scale bars show the square of the electric field strength relative to the incident field ($|E|^2/|E_0|^2$). The x – y in-plane direction is through the middle of the nanodisk height ($z = 32$ nm) and the x – z cross section is through the center of the nanodisk.

described using a Drude–Lorentz model as detailed in previous reports:^[30,58]

$$\epsilon(\lambda) = \epsilon_\infty - \frac{\omega_p^2 \tau}{\omega^2 \tau + i\omega} - \sum_j \frac{A_j}{\omega^2 - \omega_j^2 + i\omega\gamma_j} \quad (4)$$

where ϵ_∞ is the high frequency permittivity offset (beyond the measurement range). The second term is the Drude component, for which τ is the momentum-averaged scattering time, ω is the angular frequency, and ω_p is the plasma frequency. The last part of Equation (4) describes Lorentz oscillators representing other features including molecular resonances and anomalous optical conductivity behavior, where A_j , ω_j , and γ_j are amplitude, resonance angular frequency, and broadening for the j th Lorentz oscillator, respectively. Importantly, ω_p and τ are directly related to the free charge carrier density (n) and DC mobility (μ) via Equations S1 and S2 (Note B in Supporting Information). We can therefore calculate the extinction for the same nanodisks but with material permittivity corresponding to different n and/or μ .

Figure 4b shows the calculated nanodisk extinction spectra upon artificially decreasing the charge carrier density of the polymer via the Drude term of Equation (4). In the Supporting Information, we provide results of also analogously modifying the amplitudes (A_j) and broadenings (γ_j) of the Lorentz oscillator terms $\left(\sum_j \frac{A_j}{\omega^2 - \omega_j^2 + i\omega\gamma_j} \right)$ (Figure S23, Supporting

Information). In line with the experiments, the resonance peak and nano-optical response is highly suppressed with decreasing n . Our control measurements also confirm a significant drop in the charge carrier density from 100% to around 10% with applied biases (obtained from the integrated current/volume over time upon reduction of a polymer film, see Figure S24 and Table S2, Supporting Information, for details). However, the analytical calculations also suggest a significant redshift of the resonance peak position with decreasing n while the experimentally measured extinction spectra show more modest redshifts upon applying biases. Similar large calculated redshifts were also obtained if modulating both the Drude and the Lorentz oscillator terms in Equation (4) (Figure S23, Supporting Information). This discrepancy suggests that decreased charge carrier density alone does not account for the changes observed in the experimental extinction spectra. Interestingly, the analytical calculations for decreasing μ instead of n (Figure 4c) do not predict a redshift but rather a blueshift if modulating the Drude-term of Equation (4) (and hardly any shift in peak position if also modulating the Lorentz oscillators, Figure S23, Supporting Information). Reduction in the charge carrier mobility as the system reaches a reduced state may therefore complement the reduction in carrier density and contribute to the lower experimental redshift. To experimentally investigate if the mobility decreases upon reduction, we measured the conductivity (σ) of a chemically reduced PEDOT:Sulf film and estimated the mobility using $\sigma = qn\mu$, where q is the elementary

charge. Using n obtained for the electrochemically reduced film, the calculation suggests that the mobility may drop down to $\approx 1.5\%$ of the mobility of the fully oxidized plasmonic film (see Note S3, Supporting Information). Although this value may be underestimated considering that the carrier density is likely suppressed more upon chemical rather than electrochemical doping, the experiments corroborate that the tuning of the nanodisk antennas involves reduction of both carrier density and mobility. Indeed, drops in μ upon reduction has been reported previously for similar polymers, as a result of reversible changes in microstructure such as degree of order and lamellar packing distance.^[59,60] Calculated effects of simultaneously changing n and μ can be seen in Figure 4d as an overall reduction in the extinction signals with a slight redshift. Therefore, comparison of the analytical calculations with the experimental results in Figure 4a suggests that the experimental device undergoes a combined reduction of carrier density and mobility. Future work may also investigate possible influence of other variations upon reduction, including the emergence of the neutral (≈ 600 nm) and polaronic (≈ 1000 nm) peaks, which may also reduce the redshift.

Finally, we investigate effects of redox-tuning on the optical nearfields by numerically simulating the response for a single nanodisk while jointly varying both n and μ . For the fully oxidized nanodisk, we used the anisotropic complex permittivity of the original oxidized PEDOT:Sulf and then varied both the in-plane and out-of-plane permittivity via n and μ using the approach described above. As seen in Figure 4e–h, gradual reductions in n and μ from 100% (oxidized), to 70%, 30%, and 1% (reduced), greatly decreases the strength of the plasmon-enhanced fields on the opposite edges of the nanodisk. In its oxidized (plasmonic) state, the nanodisk exhibits a clear dipolar nearfield profile with enhanced fields, which then gradually decreases and disappears as n and μ decrease. The corresponding simulated extinction profiles are also consistent with this finding (Figure S25, Supporting Information).

3. Conclusion

We have demonstrated electrically tunable PEDOT:Sulf conducting polymer optical nanoantennas. The polymeric nanoantennas provide repeated on/off switching as well as reversible gradual tuning of their nano-optical response. The behavior stems from the ability to tune the polymer material between being optically metallic and dielectric. Complementary analytical calculations and control experiments show that the redox-tuning involves gradual modulation of both density and mobility of the polaronic charge carriers in the polymer. Further simulations reveal the possibility to modulate also the optical nearfield response of the nanoantennas. The concept takes important steps toward electrically tunable metasurfaces based on optical nanoantennas with electrically tunable behavior. Excitingly, this possibility was indeed confirmed by an independent study during the publication process of our manuscript, based on conducting polymer nanoantennas made of PEDOT doped with polystyrene sulfonate.^[60]

4. Experimental Section

Thin-Film Deposition: Glass substrates (7.2×2.5 cm²) were cleaned by sequential ultrasonication in a Hellmanex solution in deionized (DI) water, DI water, acetone, and isopropanol for 15 min, respectively, followed by air drying with nitrogen. The glass substrates were then put inside a Vaksis PVD MIDAS 3M thin-film coating system (VK-1902) to sputter 50 nm of ITO (sputtering conditions: 43% Ar, 25 °C, 32 W power). Following the sputtering process, the ITO/glass substrates were diced in half (3.6×2.5 cm²) and again cleaned by sequential ultrasonication in a Hellmanex solution in DI water, DI water, acetone, and isopropanol for 15 min, respectively, followed by air drying with nitrogen. The films were finally treated with oxygen plasma at 100 W for 5 min before beginning the film deposition process. For the film deposition, PEDOT:trifluoromethanesulfonate (PEDOT:OTf) thin films were first prepared as precursors of PEDOT:Sulf films. PEDOT:OTf thin films were deposited via VPP as reported in the literature.^[61] The oxidant solution for EDOT polymerization was prepared by mixing 0.03 g of iron(III) trifluoromethanesulfonate 90% (Fe(OTf)₃, Sigma Aldrich), 0.2 g of the triblock copolymer poly(ethylene glycol)-*block*-poly(propylene glycol)-*block*-poly(ethylene glycol) (average $M_n \approx 5800$, Sigma-Aldrich), and 0.8 g of 99.5% ethanol (Solveco). Oxidant films were deposited by spin coating at 1500 rpm for 22 s onto precleaned ITO substrates. After 30 s of baking on a hotplate at 70 °C, the samples were transferred inside a heated vacuum desiccator (Vacuo-temp (SELECTA)) for the VPP of PEDOT:OTf. 100 μ L of EDOT (142.18 g mol⁻¹, Sigma-Aldrich) droplets were drop cast onto two glass substrates on a hotplate at 60 °C in the desiccator to ensure its evaporation during polymerization. After 45 min of polymerization at a static pressure of 70 mbar, the samples were taken out from the desiccator and submerged inside a Petri-dish containing ethanol for 2 h. For two times and three times VPP, 45 min of polymerization was followed by soaking in ethanol for 30 min each time. Subsequently, the samples were washed by dipping into ethanol multiple times to remove the by-products and unreacted residues, followed by air drying with nitrogen. To further enhance the electrical conductivity of the samples, we used acid treatment by soaking the samples in 0.1 M H₂SO₄ for 2 min at room temperature followed by heating the samples at 120 °C for another 10 min. On acid treatment, the OTf counterions in the PEDOT:OTf films were replaced by sulfate counterions (HSO₄⁻), which was confirmed from the removal of fluorine signals in the XPS results (Figure S26, Supporting Information).

Nanoantenna Fabrication: A modified version of colloidal lithography was used for the nanodisk array fabrication as shown in Figure S6, Supporting Information.^[62] To summarize the process, a 4 wt% poly(methyl methacrylate) (PMMA) ($M_w \approx 996000$, Sigma-Aldrich) solution in anisole (Sigma Aldrich) was spin-coated at 5000 rpm onto the PEDOT:Sulf thin films. Soft baking at 140 °C for 10 min was then applied. The samples were treated with reactive oxygen plasma (50 W, 250 mtorr) for 20 s to increase the hydrophilicity of the surface. To functionalize the PMMA surface to be positively charged, 2 wt% poly(diallyldimethylammonium chloride) (522376, Sigma-Aldrich) in DI water was drop-cast onto the film to fully cover it. After 1 min 30 s, the samples were rinsed with DI water for 40 s, followed by air drying with nitrogen. Negatively charged polystyrene nanoparticles (PS beads, 197 nm, 0.2–0.3 wt% in DI water (Microparticles GmbH, PS-ST KM56-1)) were then dropped on the samples. After 10 min, the samples coated with the PS beads were rinsed with DI water and dried with a nitrogen stream, which produced a sparse monolayer of PS beads on the PMMA/PEDOT:Sulf thin films. This was followed by reactive oxygen plasma etching (250 mtorr, 50 W) for 50–130 s, using the PS beads monolayer as the mask. Depending on the thicknesses of the PMMA and PEDOT:Sulf thin films, the time interval of etching was varied to ensure a complete removal of the PMMA and PEDOT:Sulf parts that were not covered by the mask. The samples were then placed into an acetone bath and soaked for 30 min followed by a mild sonication for 5 min and nitrogen air drying to remove the PMMA and PS beads to finally produce the PEDOT:Sulf nanodisks.

Electrochemically Tunable Nanoantenna Fabrication: The ion gel was prepared by adapting the procedure described in the literature.^[48] It entailed making a solution mixture of the copolymer poly[(vinylidene fluoride)-co-hexafluoropropylene] (PVDF-HFP, $M_n = 130\,000$, Sigma Aldrich) in acetone at a 1:7 weight ratio. The solution mixture was stirred overnight at 50 °C to ensure complete dissolution of the PVDF-HFP in acetone. The ionic liquid [EMIM⁺][TFSI⁻], Sigma Aldrich, was then added into the PVDF-HFP:acetone mixture at a 1:2 ratio and the mixture was stirred on a hotplate at 50 °C for 30 min. The ion-gel mixture was spin-coated onto the glass/ITO substrate with PEDOT:Sulf nanodisks at 1000 rpm for 1 min. The spin-coated ion gel was then directly placed on a hotplate at 60 °C for 2 h to ensure drying. Another precleaned glass/ITO substrate was then placed on top of the ion gel, with the ITO contacting the ion gel, in order to function as the top electrode used to apply biases to the ion gel. The two ITO substrates were then taped together toward the edges and clamped with crocodile clips to ensure good contact between the top ITO electrode and the ion gel before placing them in the UV-vis-NIR substrate holder.

UV-Vis-NIR Spectroscopy for Measuring Voltage-Dependent Extinction Spectra, Switching, and Chronocoulometry: The extinction spectra in the vis-NIR range (400–3300 nm) were measured using a UV-vis-NIR spectrometer (Lambda 900, Perkin Elmer Instruments). The extinction spectra include transmission losses due to both absorption and scattering. For static voltage dependent measurements, a specific voltage was applied for 3–5 min to ensure the stabilization of the current before recording the spectra. A blank spectra for the voltage dependent measurements was a sample containing everything besides the PEDOT:Sulf nanodisks, specifically: glass/ITO/ion gel/ITO/glass. For samples with PEDOT:Sulf films or nanodisks on glass/ITO substrates, glass/ITO was used as the reference. For the switching measurements, time-drive mode was used to record changes in extinction over time upon switching. The bottom ITO contact was grounded, and the top ITO contact was used to apply potentials to the substrates with a Keithley 2400. To measure the current over time with various biases, an electrochemical potentiostat was used to apply and record the changes in current over a time period of 3 min until the current stabilized.

Ellipsometry: PEI-vapor-reduced PEDOT:Sulf film deposited on a two-inch single-side-polished *c*-plane sapphire wafer was characterized under normal ambient conditions at room temperature. Spectroscopic ellipsometry data were collected by ellipsometers with different spectral ranges at two to four incident angles (UV-vis-NIR—RC2 WASE J. A. Woollam Co.: 0.8–5.9 eV at 40°, 50°, 60°, and 70°; MIR—IR-VASE J. A. Woollam Co., Inc.: 0.04–0.80 eV at 40° and 60°; and THz—an in-house built THz WASE: 0.0028–0.0040 eV at 40°, 50°, and 60°). The detailed information of the characterization can be found in our previous study.^[30,51] The obtained data were analyzed by WVASE software (J. A. Woollam Co.) and an anisotropic Drude-Lorentz model was utilized for the reduced PEDOT:Sulf film with its thickness determined by surface profiler. The extracted permittivity and corresponding fitting parameters for the reduced PEDOT:Sulf film is shown in the Figure S1 and Table S1, Supporting Information.

Electrical, Chemical, and Morphological Characterization: The sheet resistance, R_s , of the thin films was measured using a four-point probe set-up with a Signatone Pro4 S-302 resistivity stand and a Keithley 2400. The film thickness t was determined by Veeco Dimension 3100 AFM. This was used to measure the electrical conductivity of PEDOT:OTf and PEDOT:Sulf films as reported in Table S3, Supporting Information. The surface morphology of the nanodisks was obtained by Veeco Dimension 3100 AFM and the images were analyzed using Nanoscope Analysis software (Bruker). X-ray photoemission experiments were carried out using a Scienta ESCA 200 spectrometer under ultrahigh vacuum conditions at a base pressure of 1×10^{-10} mbar. The XPS measurements were done with a monochromatic Al $K\alpha$ X-ray source, which provided photons with an energy of 1486.6 eV.

Optical Numerical Simulations and Calculations: Numerical simulations of the electromagnetic response of PEDOT:Sulf nanoantennas were performed via the finite-difference time-domain (FDTD) method using the commercial software Lumerical FDTD

Solutions (<http://www.lumerical.com/fdtd.php>). The optical parameters for the oxidized and chemically reduced PEDOT:Sulf thin films were taken as the anisotropic complex permittivity obtained from ellipsometry measurements. For periodic nanodisk arrays and thin films, the spectra and near-field profiles were recorded via field and power monitors. Periodic PEDOT:Sulf nanodisk arrays (or thin film) were placed on top of glass substrates. The structures were illuminated by a plane wave light source at normal incidence. Antisymmetrical and symmetrical boundaries were used for the x axis (parallel to the polarization) and y axis (normal to the polarization) and perfectly matched layers were used for the z axis (parallel to the light incident direction). For single nanodisks, the spectra were obtained using a total field/scattered field method and by extracting the extinction cross section of isolated PEDOT:Sulf nanodisks on a glass substrate. Geometry parameters were indicated in each graph (diameter, thickness, and/or array period) and the mesh size was $1 \times 1 \times 1 \text{ nm}^3$. The optical parameter for glass^[30] were taken from the literature for the simulations in Figures 1 and 2 and set to $n = 1.5$ for the other results. Permittivities of PEDOT:Sulf was determined by ellipsometry, with the values for the oxidized material taken from our previous study.^[30] In the analytical calculations, the effective permittivity of the surroundings was calculated based on an average refractive index of ion gel and glass ($\epsilon_s = [(n_{\text{iongel}} + n_{\text{glass}})/2]^2$).

Supporting Information

Supporting Information is available from the Wiley Online Library or from the author.

Acknowledgements

The authors acknowledge financial support from the Knut and Alice Wallenberg Foundation, the Swedish Research Council (VR, 2020-00287), the Swedish Foundation for Strategic Research (SSF), and the Swedish Government Strategic Research Area in Materials Science on Functional Materials at Linköping University (Faculty Grant SFO-Mat-LiU No 2009 00971). M.P.J. is a Wallenberg Academy Fellow. The authors would like to thank Dr. Dan Zhao, Dr. Debashree Banerjee, and Dr. Ludovico Migliaccio for helpful discussions.

Conflict of Interest

The authors declare no conflict of interest.

Data Availability Statement

The data that support the findings of this study are available from the corresponding author upon reasonable request.

Keywords

conducting polymers, dynamic plasmonic nanoantennas, electrical tuning, tunable metasurfaces

Received: September 9, 2021

Revised: January 14, 2022

Published online:

[1] L. Novotny, N. van Hulst, *Nat. Photonics* **2011**, *5*, 83.

- [2] X. Shi, K. Ueno, T. Oshikiri, Q. Sun, K. Sasaki, H. Misawa, *Nat. Nanotechnol.* **2018**, *13*, 953.
- [3] H. A. Atwater, A. Polman, *Nat. Mater.* **2010**, *9*, 205.
- [4] M. T. Sheldon, J. van de Groep, A. M. Brown, A. Polman, H. A. Atwater, *Science* **2014**, *346*, 828.
- [5] F. Yesilkoy, R. A. Terborg, J. Pello, A. A. Belushkin, Y. Jahani, V. Pruner, H. Altug, *Light: Sci. Appl.* **2018**, *7*, 17152.
- [6] F. Mazzotta, G. Wang, C. Hägglund, F. Höök, M. P. Jonsson, *Biosens. Bioelectron.* **2010**, *26*, 1131.
- [7] M. P. Jonsson, A. B. Dahlin, P. Jönsson, F. Höök, *Biointerphases* **2008**, *3*, FD30.
- [8] M. P. Jonsson, P. Jönsson, A. B. Dahlin, F. Höök, *Nano Lett.* **2007**, *7*, 3462.
- [9] P. Englebienne, *Analyst* **1998**, *123*, 1599.
- [10] L. Shao, X. Zhuo, J. Wang, *Adv. Mater.* **2018**, *30*, 1704338.
- [11] D. Franklin, R. Frank, S.-T. Wu, D. Chanda, *Nat. Commun.* **2017**, *8*, 15209.
- [12] K. Xiong, G. Emilsson, A. Maziz, X. Yang, L. Shao, E. W. H. Jager, A. B. Dahlin, *Adv. Mater.* **2016**, *28*, 9956.
- [13] K. Xiong, D. Tordera, M. P. Jonsson, A. B. Dahlin, *Rep. Prog. Phys.* **2019**, *82*, 024501.
- [14] J. Park, J.-H. Kang, S. J. Kim, X. Liu, M. L. Brongersma, *Nano Lett.* **2017**, *17*, 407.
- [15] X. Chen, L. Huang, H. Mühlenbernd, G. Li, B. Bai, Q. Tan, G. Jin, C.-W. Qiu, S. Zhang, T. Zentgraf, *Nat. Commun.* **2012**, *3*, 1198.
- [16] F. Aieta, P. Genevet, M. A. Kats, N. Yu, R. Blanchard, Z. Gaburro, F. Capasso, *Nano Lett.* **2012**, *12*, 4932.
- [17] J. B. Pendry, *Phys. Rev. Lett.* **2000**, *85*, 3966.
- [18] N. Yu, P. Genevet, M. A. Kats, F. Aieta, J.-P. Tetienne, F. Capasso, Z. Gaburro, *Science* **2011**, *334*, 333.
- [19] G. V. Naik, V. M. Shalae, A. Boltasseva, *Adv. Mater.* **2013**, *25*, 3264.
- [20] Y. Wang, P. Landreman, D. Schoen, K. Okabe, A. Marshall, U. Celano, H.-S. P. Wong, J. Park, M. L. Brongersma, *Nat. Nanotechnol.* **2021**, *16*, 667.
- [21] R. Alaei, M. Albooyeh, S. Tretyakov, C. Rockstuhl, *Opt. Lett.* **2016**, *41*, 4099.
- [22] M. Wuttig, H. Bhaskaran, T. Taubner, *Nat. Photonics* **2017**, *11*, 465.
- [23] Y. Kim, P. C. Wu, R. Sokhoyan, K. Mauser, R. Glauddell, G. K. Shirmanesh, H. A. Atwater, *Nano Lett.* **2019**, *19*, 3961.
- [24] S. Abdollahramezani, O. Hemmatyar, H. Taghinejad, A. Krasnok, Y. Kiarashinejad, M. Zandehshahvar, A. Alù, A. Adibi, *Nanophotonics* **2020**, *9*, 1189.
- [25] Z. Liu, Y. Zhong, I. Shafei, R. Borman, S. Jeong, J. Chen, Y. Losovyj, X. Gao, N. Li, Y. Du, E. Sarnello, T. Li, D. Su, W. Ma, X. Ye, *Nat. Commun.* **2019**, *10*, 1394.
- [26] Z. Fang, S. Thongrattanasiri, A. Schlather, Z. Liu, L. Ma, Y. Wang, P. M. Ajayan, P. Nordlander, N. J. Halas, F. J. García de Abajo, *ACS Nano* **2013**, *7*, 2388.
- [27] H. Yan, X. Li, B. Chandra, G. Tulevski, Y. Wu, M. Freitag, W. Zhu, P. Avouris, F. Xia, *Nat. Nanotechnol.* **2012**, *7*, 330.
- [28] L. Ju, B. Geng, J. Horng, C. Girit, M. Martin, Z. Hao, H. A. Bechtel, X. Liang, A. Zettl, Y. R. Shen, F. Wang, *Nat. Nanotechnol.* **2011**, *6*, 630.
- [29] J. R. Reynolds, B. C. Thompson, T. A. Skotheim, *Conjugated Polymers: Properties, Processing, and Applications*, CRC Press, Boca Raton, FL, USA **2019**.
- [30] S. Chen, E. S. H. Kang, M. S. Chaharsoughi, V. Stanishev, P. Kühne, H. Sun, C. Wang, M. Fahlman, S. Fabiano, V. Darakchieva, M. P. Jonsson, *Nat. Nanotechnol.* **2020**, *15*, 35.
- [31] Y. R. Leroux, J. C. Lacroix, K. I. Chane-Ching, C. Fave, N. Félidj, G. Lévi, J. Aubard, J. R. Krenn, A. Hohenau, *J. Am. Chem. Soc.* **2005**, *127*, 16022.
- [32] Y. Kim, S. Cha, J.-H. Kim, J.-W. Oh, J.-M. Nam, *Nanoscale* **2021**, *13*, 9541.
- [33] W. Lu, N. Jiang, J. Wang, *Adv. Mater.* **2017**, *29*, 1604862.
- [34] J. Peng, H.-H. Jeong, Q. Lin, S. Cormier, H.-L. Liang, M. F. L. De Volder, S. Vignolini, J. J. Baumberg, *Sci. Adv.* **2019**, *5*, eaaw2205.
- [35] H. Huang, W. Feng, Y. Chen, *Chem. Soc. Rev.* **2021**, *50*, 11381.
- [36] B. J. Bohn, M. Schnell, M. A. Kats, F. Aieta, R. Hillenbrand, F. Capasso, *Nano Lett.* **2015**, *15*, 3851.
- [37] Y. Ke, Y. Yin, Q. Zhang, Y. Tan, P. Hu, S. Wang, Y. Tang, Y. Zhou, X. Wen, S. Wu, T. J. White, J. Yin, J. Peng, Q. Xiong, D. Zhao, Y. Long, *Joule* **2019**, *3*, 858.
- [38] I. Zozoulenko, A. Singh, S. K. Singh, V. Gueskine, X. Crispin, M. Berggren, *ACS Appl. Polym. Mater.* **2019**, *1*, 83.
- [39] G. Sonmez, *Chem. Commun.* **2005**, 5251.
- [40] J. G. Ibanez, M. E. Rincón, S. Gutierrez-Granados, M. Chahma, O. A. Jaramillo-Quintero, B. A. Frontana-Urbe, *Chem. Rev.* **2018**, *118*, 4731.
- [41] N. Massonnet, A. Carella, A. de Geyer, J. Faure-Vincent, J.-P. Simonato, *Chem. Sci.* **2014**, *6*, 412.
- [42] J. Rivnay, S. Inal, A. Salleo, R. M. Owens, M. Berggren, G. G. Malliaras, *Nat. Rev. Mater.* **2018**, *3*, 17086.
- [43] D. Kim, H. Jang, S. Lee, B. J. Kim, F. S. Kim, *ACS Appl. Mater. Interfaces* **2021**, *13*, 1065.
- [44] B. Hasse, J. Lehmann, D. Assenbaum, P. Wasserscheid, A. Leipertz, A. P. Fröba, *J. Chem. Eng. Data* **2009**, *54*, 2576.
- [45] J. M. Porter, C. B. Dreyer, D. Bicknese, S. Vyas, C. M. Maupin, J. Poshusta, J. Martin, *J. Quant. Spectrosc. Radiat. Transfer* **2014**, *133*, 300.
- [46] S. Desai, R. L. Shepherd, P. C. Innis, P. Murphy, C. Hall, R. Fabretto, G. G. Wallace, *Electrochim. Acta* **2011**, *56*, 4408.
- [47] D. Zhao, A. Martinelli, A. Willfahrt, T. Fischer, D. Bernin, Z. U. Khan, M. Shahi, J. Brill, M. P. Jonsson, S. Fabiano, X. Crispin, *Nat. Commun.* **2019**, *10*, 1093.
- [48] C. Cendra, A. Giovannitti, A. Savva, V. Venkatraman, I. McCulloch, A. Salleo, S. Inal, J. Rivnay, *Adv. Funct. Mater.* **2019**, *29*, 1807034.
- [49] K. Xiong, O. Olsson, J. Svirelis, J. Baumberg, A. Dahlin, *Adv. Mater.* **2021**, *33*, 2103217.
- [50] R. Brooke, M. Fabretto, M. Krasowska, P. Talemi, S. Pering, P. J. Murphy, D. Evans, *J. Mater. Chem. C* **2016**, *4*, 1550.
- [51] S. Chen, S. Rossi, R. Shanker, G. Cincotti, S. Gamage, P. Kühne, V. Stanishev, I. Engquist, M. Berggren, J. Edberg, V. Darakchieva, M. P. Jonsson, *Adv. Mater.* **2021**, *33*, 2102451.
- [52] J. Kawahara, P. A. Ersman, I. Engquist, M. Berggren, *Org. Electron.* **2012**, *13*, 469.
- [53] P. Tehrani, L.-O. Hennerdal, A. L. Dyer, J. R. Reynolds, M. Berggren, *J. Mater. Chem.* **2009**, *19*, 1799.
- [54] S. A. Maier, *Plasmonics: Fundamentals and Applications*, Springer Science & Business Media, New York **2007**.
- [55] A. Wokaun, J. P. Gordon, P. F. Liao, *Phys. Rev. Lett.* **1982**, *48*, 957.
- [56] C. Langhammer, Z. Yuan, I. Zorić, B. Kasemo, *Nano Lett.* **2006**, *6*, 833.
- [57] S. Chen, P. Kühne, V. Stanishev, S. Knight, R. Brooke, I. Petsagkourakis, X. Crispin, M. Schubert, V. Darakchieva, M. P. Jonsson, *J. Mater. Chem. C* **2019**, *7*, 4350.
- [58] B. D. Paulsen, R. Wu, C. J. Takacs, H.-G. Steinrück, J. Strzalka, Q. Zhang, M. F. Toney, J. Rivnay, *Adv. Mater.* **2020**, *32*, 2003404.
- [59] E. M. Thomas, M. A. Brady, H. Nakayama, B. C. Popere, R. A. Segalman, M. L. Chabiny, *Adv. Funct. Mater.* **2018**, *28*, 1803687.
- [60] J. Karst, M. Floess, M. Ubl, C. Dingler, C. Malacrida, T. Steinle, S. Ludwigs, M. Hentschel, H. Giessen, *Science* **2021**, *374*, 612.
- [61] R. Brooke, J. F. Franco-Gonzalez, K. Wijeratne, E. Pavlopoulou, D. Galiani, X. Liu, R. Valiollahi, I. V. Zozoulenko, X. Crispin, *J. Mater. Chem. A* **2018**, *6*, 21304.
- [62] P. Hanarp, M. Käll, D. S. Sutherland, *J. Phys. Chem. B* **2003**, *107*, 5768.